Accepted Manuscript

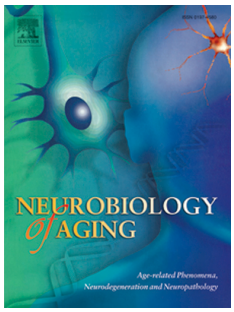

Early hippocampal hyper-excitability in PS2APP mice: role of mutant PS2 and APP

Roberto Fontana, Mario Agostini, Emanuele Murana, Mufti Mahmud, Elena Scremin, Maria Rubega, Giovanni Sparacino, Stefano Vassanelli, Cristina Fasolato

PII: S0197-4580(16)30278-0

DOI: 10.1016/j.neurobiolaging.2016.10.027

Reference: NBA 9766

To appear in: *Neurobiology of Aging*

Received Date: 11 June 2016

Revised Date: 17 October 2016

Accepted Date: 28 October 2016

Please cite this article as: Fontana, R., Agostini, M., Murana, E., Mahmud, M., Scremin, E., Rubega, M., Sparacino, G., Vassanelli, S., Fasolato, C., Early hippocampal hyper-excitability in PS2APP mice: role of mutant PS2 and APP, *Neurobiology of Aging* (2016), doi: 10.1016/j.neurobiolaging.2016.10.027.

This is a PDF file of an unedited manuscript that has been accepted for publication. As a service to our customers we are providing this early version of the manuscript. The manuscript will undergo copyediting, typesetting, and review of the resulting proof before it is published in its final form. Please note that during the production process errors may be discovered which could affect the content, and all legal disclaimers that apply to the journal pertain.

ACCEPTED MANUSCRIPT

TITLE PAGE

Early hippocampal hyper-excitability in PS2APP mice: role of mutant PS2 and APP

AUTHOR NAMES

Roberto Fontana[a], Mario Agostini[a], Emanuele Murana[a1], Mufti Mahmud[a], Elena Scremin[a], Maria Rubega[b], Giovanni Sparacino[b], Stefano Vassanelli[a†] and Cristina Fasolato[a†].

AFFILIATIONS

[a] Department of Biomedical Sciences, University of Padova, Via Ugo Bassi 58/B, 35131 Padova, Italy

[b] Department of Information Engineering, University of Padova, Via G. Gradenigo 6/B, 35131 Padova, Italy

[†] Corresponding authors

[1] Present address: Department of Neuroscience, Biomedicine and Movement Sciences, Section of Anatomy and Histology, University of Verona, Strada le Grazie 8, 37131 Verona, Italy

E-MAIL ADDRESSES:

Roberto Fontana, roberto.fontana@unipd.it; Mario Agostini, mario.agostini@phd.unipd.it; Emanuele Murana, emanuele.murana@univr.it; Mufti Mahmud, mufti.mahmud@unipd.it; Elena Scremin, elena.scremin@studenti.unipd.it; Maria Rubega, maria.rubega@phd.unipd.it; Giovanni Sparacino, giovanni.sparacino@unipd.it; Stefano Vassanelli, stefano.vassanelli@unipd.it; Cristina Fasolato, cristina.fasolato@unipd.it

Abbreviations: cross-frequency coupling (CFC), phase-amplitude CFC (PAC), general linear model (GLM), power spectral density (PSD), slow oscillations (SO), slow Gamma (SG), fast Gamma (FG).

ACCEPTED MANUSCRIPT

ABSTRACT

Alterations of brain network activity are observable in Alzheimer's disease (AD) together with the occurrence of mild cognitive impairment, before overt pathology. However, in humans as well in AD mouse models identification of early biomarkers of network dysfunction is still at its beginning. We performed in vivo recordings of local field potential (LFP) activity in the dentate gyrus (DG) of PS2APP mice expressing the human amyloid precursor protein (APP) Swedish mutation and the presenilin-2 (PS2) N141I. From a frequency-domain analysis, we uncovered network hyper-synchronicity as early as 3 months, when intracellular accumulation of amyloid-beta (Aβ) was also observable. Additionally, at 6 months of age, we identified network hyper-activity in the Beta/Gamma frequency bands, along with increased Theta-Beta and Theta-Gamma phase-amplitude cross-frequency coupling (CFC), in coincidence with the histo-pathological traits of the disease. Whereas hyper-activity and hyper-synchronicity were respectively detected in mice expressing the PS2-N141I or the APP Swedish mutant alone, the increase in CFC specifically characterized the 6-month-old PS2APP mice, just before the surge of the cognitive decline.

Keywords: Alzheimer's disease, local field potential, dentate gyrus, PS2APP, hyper-excitability, amyloid-beta

ACCEPTED MANUSCRIPT

1 INTRODUCTION

Alzheimer's disease (AD) is a neurodegenerative pathology that affects an increasing number of elderly people. It is characterized by progressive impairment in cognition and memory and it is the most frequent cause of dementia, being responsible for 60 to 70 % of the cases over 65 years (World Health Organization, 2015). After the failure of Aβ-targeting therapies in clinical trials, one possible explanation is the fact that the treated patients had already fully developed the disease, as revealed by combined fMRI and cognitive assessment (Golde et al., 2011). These discouraging results highlight the urgency of early biomarkers that reliably indicate the undercover developing disease and that predict the overt onset of the first clinical symptoms with years of advance. From this perspective, PET/CSF and brain volumetric biomarkers proved to be valuable tools for predicting MCI to AD conversion over 2 years (Mitchell et al., 2010). Yet, the moment when the brain has already started to shrink is anyhow likely to be very late, implying that a hypothetically effective disease-modifying therapy would yield no appreciable improvement because of the other detrimental mechanisms that have, meanwhile, established. Likewise, alterations in oscillatory brain activity were assessed in subjects already presenting symptoms of cognitive decline (Bhat et al., 2015).

AD mouse models provide the possibility to address potential changes of brain network activity that precede amyloid deposition and cognitive defects. Ca^{2+} hyper-activity and hyper-excitability appear to be among the first alterations observable at the brain level (Stargardt et al., 2015). Dysregulation of Ca^{2+} signaling, which is closely linked to mitochondrial dysfunction and ROS formation, has been implicated in the aged and diseased brain (Agostini and Fasolato, 2016, Decuypere et al., 2011) and consistently reported in different AD mouse models (Busche et al., 2015, Busche et al., 2012, Camandola and Mattson, 2011, Kipanyula et al., 2012, Stargardt et al., 2015, Zampese et al., 2011a). A FAD-linked mutation in PS2 has been shown to cause profound alteration of Ca^{2+} signaling in fibroblasts obtained from FAD patients, well before the onset of the cognitive decline (Giacomello et al., 2005). Other FAD-linked PS2 mutations show similar Ca^{2+} defects (Kipanyula et al., 2012, Zampese et al., 2011b, Zatti et al., 2006). Recently, early neuronal impairment of Ca^{2+} homeostasis has been described in AD mouse models based on PS2-N141I, with increased Ca^{2+} excitability proved both *in vitro* and *in situ* (Kipanyula et al., 2012). Thus, we reasoned that addressing hyper-activity due to Ca^{2+} as well as Aβ dysregulation, brought about by mutant PS2 in young

mice, might help defining early markers of disease progression. In particular, we asked whether and from which stage of the disease it is possible to detect early network dysfunctions in the homozygous AD mouse line PS2APP (B6.152H), expressing the hPS2-N141I in the presence of the hAPP Swedish mutation (hAPPSwe) (Kipanyula et al., 2012, Ozmen et al., 2009, Richards et al., 2003). While the C57BL/6J mice were regularly used as a control, a comparison was also carried out with other homozygous mouse lines, the PS2-NI (PS2.30H) and the hAPPSwe (BD.AD147.72H) lines, expressing either the PS2-N141I or the hAPPSwe, respectively (Richards et al., 2003), and the PS2 knockout (PS2KO) mouse line (Herreman et al., 1999).

By recording *in vivo* the spontaneous LFP activity in the DG of mice under urethane anesthesia, we investigated the brain oscillatory activity in terms of power spectral density (PSD) and phase-amplitude CFC (PAC). Of note, PS2APP mice were analyzed before and after the onset of Aβ deposition and gliosis, and compared to age-matched control and single transgenic (tg) mice. To our knowledge, only few studies have addressed spontaneous hippocampal oscillatory activity in AD mouse models in vivo at the early stages of the disease (Born et al., 2014, Ittner et al., 2014, Verret et al., 2012, Xu et al., 2015). Importantly, this is the first study addressing the role of PS2 on brain excitability in AD tg mouse models.

2 METHODS

2.1 ANIMALS

The homozygous tg mouse lines PS2APP (B6.152H) and APPSwe (BD.AD147.72H) were kindly donated by L. Ozmen (F. Hoffmann-La Roche Ltd, Basel, Switzerland) (Richards et al. 2003; Ozmen et al., 2009). The homozygous tg lines PS2-NI (PS2.30H) (Ozmen et al., 2009) and PS2KO (Herreman, et al. 1999) were obtained by embryo revitalization from Charles River Laboratories (CRL, Lecco, Italy) and CNR-EMMA repository (Rome, Italy), respectively. In these lines, APP and PSEN2 transgenes are driven by mouse Thy-1 and mouse prion promoters, respectively. All lines were originally backcrossed to C57BL/6J (wt) mice for 4 or more generations, the resulting backgrounds are reported in Supplementary Table 1. As a control, we used a wt colony established in our SPF animal facility from littermates obtained following PS2-NI backcrossing. For all lines, inbreeding was avoided and age-matched females were used without checking estrous cycle. Specific work on similar type of recordings (Gurevicius et al., 2013) and meta-analysis studies (Prendergast et al., 2014) indicate that estrous cycle does not increase female variability. All experimental

procedures were carried out in strict adherence to the Italian regulations on animal protection and care and with the explicit approval of the Italian animal welfare regulations (Decreto autorizzativo 447/2015-PR).

Acute animal preparation. Female mice were anesthetized by intraperitoneal injection of urethane (1.5-2 mg/g, U2500 - Sigma-Aldrich) dissolved in 0.9% NaCl physiological saline. An initial dose of 1.2 mg/g was injected and additional doses (0.15 mg/g) were administered when required (Namgung et al., 1995). Absence of reaction to noxious stimuli (e.g. hind paw pinches) ensured the surgical plane of anesthesia. Body temperature was kept at 37 ± 0.5°C by means of a servo-controlled heating pad (ATC1000 – World Precision Instruments, Inc.). Krebs solution (0.1 ml) was subcutaneously administered every two hours in order to maintain hydration levels. The head was restrained in a stereotaxic frame and the skull was exposed. A hole was drilled at the site for inserting the recording electrode in the DG which was located about 2.4 mm posterior to bregma and 1.2 mm lateral to midline (Huang et al., 2012). The left hemisphere was selected provided that amyloid plaques deposition is stronger in this hemisphere (Khan et al., 2014). The cavity over the skull was filled with Krebs saline solution and a silver chloride reference electrode was dipped within. Glass electrodes for LFP recording (0.9-1.6 MΩ tip resistance) were obtained from borosilicate capillaries (GB150T-10 – Science Products GmbH) pulled with a P-97 micropipette puller (Sutter Instrument Company) and filled with Krebs solution. In each animal, the LFP signal was serially acquired at three different depths from the meninges: 1.7, 1.8 and 1.9 mm. These depths correspond to the molecular layer, the granule cell layer and the polymorphic layer of the DG.

Heart beat was monitored through electrocardiogram (ECG) recording. ECG positive and negative derivations were subcutaneously inserted in the forelimbs. A high accuracy temperature probe was leaned against the chest wall, on the side of the body, to monitor respiration (IT-23, World Precision Instruments). At the end of the electrophysiological experiment, mice were euthanized by excess of anesthesia and the brain was dissected. The left hemisphere was intended for histological investigations and was fixed in 4% paraformaldehyde [PFA) in Tris-buffer saline, TBS: NaCl (150 mM), Tris (50 mM), pH adjusted to 7.4 with HCl]. Conversely, the right-hemisphere cortex and hippocampus were snap-frozen in liquid nitrogen for biochemical assays.

2.2 ELECTROPHYSIOLOGY

Data acquisition. The LFP signal was 10X amplified using an Axoclamp-2B amplifier with an HS-2Ax1LU headstage (Axon Instruments Inc.) in bridged mode. A custom-made amplifier provided further 10X amplification along with 4-pole butterworth low-pass filtering at 1 kHz. The ECG signal was 10X amplified and band-passed between 1 and 100 Hz by means of a DAM50 amplifier (World Precision Instruments). Respiration-induced movements of the chest wall were converted in voltage fluctuation by exploiting the piezoelectric properties of the temperature probe. Respiration signal was 100X amplified and band-passed between 0.1 and 100 Hz by means of a DP-301 amplifier (Warner Instruments). Signals were digitalized at 10 kHz by means of a PCI-6071E I/O card (-0.5 – 0.5 V input range) combined with a BNC-2090 terminal block (National Instruments) in differential mode and recorded through a custom-made LabView (National Instruments) script. Each recording lasted 15 minutes on average. See Supplementary Methods for electrophysiological data analysis.

2.3 IMMUNOHISTOCHEMISTRY

Mid-sagittal brain slices were cut from the left hemisphere and conserved in TBS at 4 °C until employed for dorsal hippocampus immunostaining. For staining, floating slices were selected over a range of 400 µm. First, Slices, washed in TBS and incubated for 5 minutes in 70% formic acid, were incubated in blocking buffer containing 0.3% TritonX-100 and 5% goat serum in TBS for 1 hour at room temperature (RT). Next, they were incubated overnight at 4°C with mouse anti-Aβ 17-24 (4G8, Covance, 1:1000) and rabbit anti-GFAP (Dako, 1:400). Then, slices were incubated, for 1 h at RT in the dark, with donkey anti-rabbit Alexa488 (Invitrogen, 1:1000) and goat anti-mouse Alexa555 (Invitrogen, 1:1000). Mowiol-mounted slices were stored at 4°C until visualization by means of Leica SP5 (20X). For astrogliosis quantification, we considered the average brightness level of GFAP labelling in the HF region. In each image, a region of interest (ROI) was traced encompassing the following regions: subiculum, DG, CA3 and CA1; for the cortex, a rectangular ROI of invariant size was drawn. Then, the average 8-bit pixel intensity (0-255) was computed for each ROI. Three slices for each mouse (n=3 mice per line) were used to quantify the mean average value of the selected regions (Fiji). Slices from the wt, PS2-NI, PS2APP and/or APPSwe mice were processed in parallel.

2.4 STATISTICAL ANALYSES

Statistical analyses were carried out in Prism (GraphPad). Power spectra, band power, PSD slope, PSD offset and PAC indices, obtained from the recordings at the three depths, were averaged within animals to obtain grand mean quantifications for each animal. Differences among means were tested by performing Kruskal-Wallis nonparametric test. Where Kruskal-Wallis test resulted in the existence of a pair of different populations, differences between means where tested with Mann-Whitney Rank Sum test. Correlation between variables was assessed by means of the Spearman's rank correlation coefficient. The unpaired two-tailed Mann-Whitney Rank Sum test was employed for mean brightness intensities. All data are expressed as mean ± SEM. The α level of significance was 0.05 (*$p < 0.05$; ** $p<0.01$; *** $p< 0.001$; **** $p<0.0001$).

3 RESULTS

3.1 IN VIVO LFP RECORDINGS IN THE DG OF PS2-BASED AD MICE

Compelling evidence was provided for dysregulation of neuronal Ca^{2+} homeostasis along with network Ca^{2+} hyper-activity in hippocampal slices from 2-week-old PS2APP and PS2-NI mice (Kipanyula et al., 2012). In order to address *in vivo* the existence of alterations in network activity, we recorded spontaneous hippocampal LFPs from the DG of wt, PS2-NI and PS2APP mice at 3, 6 and 12 months of age, under urethane anesthesia (Supplementary Fig. 1 and Methods). To keep the groups more homogeneous, only female mice were considered given the fact that, in females, anticipation of the pathology characterizes the disease in humans as well as PS2APP mice (Ozmen et al., 2009). All the below reported analyses are based on the following numbers of mice: 11, 8, 8 (3-month-old); 10, 12, 12 (6-month-old) and 9, 7, 9 (12-month-old) for wt, PS2-NI and PS2APP lines respectively, with a tolerance of 1 week for the 3 month-group, 2 weeks for the 6 and 4 weeks for the 12 month-groups.

3.2 POWER SPECTRAL DENSITY

We evaluated the overall neural population activity in the DG by analyzing the PSD function obtained from the LFP traces recorded during stable and regular heart and respiration rates (see Supplementary Methods and Supplementary Fig. 1). Analysis of the different frequency bands was carried out in the following

intervals: Slow Oscillations (SO, 0.1-1.4 Hz), Theta (1.7-4.7 Hz), Beta (10-25 Hz), Slow-Gamma (SG, 25-40 Hz), Fast-Gamma (FG, 45-90 Hz) and Epsilon (110-190 Hz) (Supplementary Fig. 1C). At a first glance, with respect to wt mice, the PSD plots showed a marked broad-band power increase in the range from 15 to 60 Hz, in both PS2-NI and PS2APP mice at 6 months of age but only in PS2APP mice at 3 months of age (Fig. 1, A-C). Quantification of the power within discrete frequency bands revealed that, for 6 month-old PS2-NI mice, the increase was statistically significant ($p < 0.05$, Mann-Whitney rank-sum test) in the SG (PS2-NI, 1.12e-3 ± 0.19; wt , 0.58e-3 ± 0.17e-3 mV^2) and in the FG (PS2-NI, 1.08e-3 ± 0.18e-3; wt, 0.59e-3 ± 0.19e-3 mV^2) ranges and, for 6 month-old PS2APP mice, in the Beta (PS2APP, 2.59e-3 ± 0.31e-3; wt, 1.18e-3 ± 0.32e-3 mV^2) and SG (PS2APP, 1.35e-3 ± 0.18e-3; wt, 0.58e-3 ± 0.17e-3 mV^2) ranges (Fig. 1, D-F). In these frequency bands, no alterations were observed at 12 months of age for both tg lines, whereas the remaining frequency bands (SO, Theta and Epsilon) stayed unaltered at all ages (Supplementary Fig. 3A-C).

We further investigated whether the steepness of the PSD function could also be altered, since it was shown that several neurological diseases and disturbs, including Parkinson's disease and schizophrenia, affect PSD steepness, especially in the Gamma range (Voytek and Knight, 2015). The PSD log-log plots shown in Figure 1 presented a corner frequency around 30-40 Hz, which prevented a proper linear fitting in the Gamma frequency range. The steepness of the $1/f^x$ noise function was thus estimated following linear fitting of PSD plots in the semi-log space (10-100 Hz), as previously described (Voytek et al., 2015). As shown in Figure 2, comparison of the slope coefficients revealed that the power decay was significantly steeper in PS2APP mice compared to wt at both 3 and 6 months of age (PS2APP, -0.26 ± 0.01; wt, -0.21 ± 0.01 at 3 months and PS2APP, -0.24 ± 0.01; wt, -0.20 ± 0.01 at 6 months, mean ± SEM, $p < 0.05$, Mann-Whitney rank-sum test). A tendency in the same direction, albeit not significant, was also clear at 12 months of age. In contrast, in PS2-NI mice, PSD steepness was comparable to that found in wt mice at each considered age. All in all, these results indicate an overall alteration of DG network synchronicity under urethane anesthesia, as inferable through the analysis of the PSD slope coefficient, in PS2APP, but not PS2-NI mice, as soon as 3 months of age. We also compared the PSD functions for the same genotype across different ages in the log-log and semi-log space (Supplementary Fig. 4, A-F). Upon linear fitting, as described

in the previous paragraph, we noticed that in PS2APP mice, the increase in steepness was lost at 12 months (PS2APP, -0.22 ± 0.01; wt, -0.20 ± 0.01, Supplementary Fig. 4G).

Finally, offset values were compared per genotype, across ages (Fig. 2E). Two pieces of information clearly emerged: i) at 3 and 6 months of age, PS2APP mice have a much higher offset compared to wt and PS2-NI mice (PS2APP, 7.49e-4 ± 1.32e-4; PS2-NI, 3.37e-4 ± 0.57e-4; wt, 3.75e-4 ± 0.54e-4 mV^2/Hz at 3 months and PS2APP, 4.81e-4 ± 0.65e-4; PS2-NI, 3.24e-4 ± 0.62e-4; wt, 1.50e-4 ± 0.41e-4 mV^2/Hz at 6 months; $p < 0.05$, Mann-Whitney rank-sum test); ii) in wt mice, the offset rapidly decreased with age (for a better comparison, the same data were plotted per age in Supplementary Fig. 4H, $p < 0.05$, Mann-Whitney rank-sum test), whereas the decline was delayed in PS2APP mice, and the offset showed a significant reduction only at 12 months; in PS2-NI mice, offset reduction with age was not statistically significant.

3.3 Phase Amplitude Coupling

In addition to the analysis of the spectral changes, we considered another feature of brain LFP signals that are nested oscillations, where a slower rhythm influences a faster one in a dynamic fashion. We asked whether the spectral alterations that we observed could be accompanied by changes in CFC - i.e. the relationship within each pair of nested oscillations - between the phase of one oscillation and the amplitude of a higher frequency. We quantified the PAC in the Theta-Beta, -SG, -FG and -Epsilon classes by computing the General Linear Model (GLM) index (Penny et al., 2008) (Supplementary Methods).

In PS2APP mice at 6 months of age, the pattern of alteration of the PAC level in the different classes closely resembled that of power (Fig. 1D, E & Fig. 3A, B). In fact, compared to wt mice, PAC resulted significantly enhanced for both the Theta-Beta (PS2APP, 0.17 ± 0.02; wt, 0.10 ± 0.01) and the Theta-SG range (PS2APP, 0.21 ± 0.03; wt, 0.13 ± 0.02, $p < 0.05$, Mann-Whitney rank-sum test). In contrast, PS2-NI mice did not present any significant difference in the PAC level ($p \geqslant 0.05$, Mann-Whitney rank-sum test) with respect to wt mice, either at 3 or 6 months of age. Despite the increase of SG and FG power in 6-month-old PS2-NI mice, the level of PAC in the classes concerning those bands resulted unaffected. Finally, only the PS2APP mice reported a significant reduction of Theta-Epsilon PAC at 12 months (PS2APP, 0.10 ± 0.01; wt, 0.15 ± 0.01) (Fig. 3D).

Interestingly, following Spearman rank correlation analysis, offset values significantly correlated with power ($p < 0.05$, permutation test), particularly in the Gamma range for all genotypes (Supplementary Fig. 5A), reinforcing the notion that PSD offset reflects local population spiking activity (Voytek and Knight, 2015). Theta-SG PAC significantly correlated with Theta, yet not SG (Supplementary Fig. 5D, E), nor FG power (data not shown). Further, a significant correlation was also found between Theta-SG PAC and steepness only for the PS2APP line (Supplementary Fig. 5F).

3.4 Amyloid beta accumulation and astrogliosis

Among the major histo-pathological hallmarks of AD are the extracellular deposition of amyloid plaques and the establishment of gliosis, i.e. the sustained inflammatory glial response to insulting conditions. We evaluated the deposition of amyloid plaques as well as the presence of astrogliosis by IHC (see Methods) in hippocampal slices of PS2APP, PS2-NI and wt mice at 3 and 6 months of age, in correspondence with the main electrophysiological traits emerged from our analysis.

We consistently found marked plaque deposition in the hippocampal formation (HF), especially in the *subiculum* and, to a lesser degree, in the DG, as well as in the cerebral cortex of 6-month-old PS2APP mice when compared to age-matched wt mice (Fig. 4A, C, left). These findings confirm and expand previous observations obtained in the brain of PS2APP mice by the Congo red approach, which primarily detects the fibrillary deposits (Ozmen et al., 2009). In contrast, extracellular amyloid aggregates were not observed in PS2-NI mice at this age (Fig. 4B, left), as well as at 12 months (data not shown). In 3 month-old PS2APP mice, however, a noticeable intracellular amyloid staining was detected in all considered territories (Fig. 5A), yet it was particularly strong in the *subiculum* (Fig. 5B) and in the pyramidal layer (sp, *stratum pyramidalis*) of the CA1 region, with a clear granular appearance (Fig. 5C). Interestingly, early detection of a strong intra-neuronal Aβ/APP signature that fades at subsequent ages has been previously reported in other AD mouse models based on mutant APP (Lord et al., 2006, Zou et al., 2015).

In AD, astrocytes become reactive and increase the expression levels of the intermediate filament protein GFAP, a condition known as astrogliosis (Steardo Jr et al., 2015). We detected the GFAP expression level in hippocampal slices adjacent to those used for APP/Aβ detection (Fig. 4A-C, right). A quantitative analysis was carried out within specific regions, as defined in Methods and summarized in Figure 4D. We found a

statistically significant increase of mean intensity ($p < 0.05$, Mann-Whitney rank-sum test) in 6-month-old PS2APP mice, compared to age-matched wt mice, in *subiculum* (+ 44.2%), DG (+ 37.0%) and cortex (+ 42.4%).

It is largely accepted that synaptic loss and neuronal dysfunction in AD are mainly caused by accumulation of soluble forms of $A\beta_{42}$, especially small oligomers, rather than by amyloid plaques. The accumulation of $A\beta_{42}$ was thus evaluated at the hippocampal level by means of ELISA kits suited to measure both mouse and human $A\beta_{42}$ (see Methods). As shown in Supplementary Figure 6, in wt and PS2-NI mice, $A\beta_{42}$ levels were comparable at any age, being in the order of few pg/mg of wet tissue (n = 3 mice, each group). In contrast, compared to wt, the PS2APP mice showed a dramatic increase in $A\beta_{42}$ levels, at both 3 and 6 months of age, being respectively 10^2 and 10^3 times the wt level. Between 6 and 12 months of age, the $A\beta_{42}$ load continued to grow, yet at a lower rate, a result in agreement with previous observations (Ozmen et al., 2009). These results identify the 3-6 month-period as the exponential phase of $A\beta$ accumulation in PS2APP mice. $A\beta_{40}$ accumulates in a similar way being the $A\beta_{42}/A\beta_{40}$ ratio close to 1 in this mouse model, at any age ((Ozmen et al., 2009) and Supplementary Table 1.

3.5 Role of PS2 and APP

ACCEPTED MANUSCRIPT

Table 1. Summary of the electrophysiological alterations in the tg mouse lines in comparison with wt mice.

	3 months		6 months				12 months	
	PS2-NI	PS2APP	PS2-NI	PS2APP	PS2KO	APPSwe	PS2-NI	PS2APP
Beta power	-	-	-	↑↑	-	-	-	-
SG power	-	-	↑	↑↑	-	-	-	-
FG power	-	-	↑	-	-	-	-	-
Theta-beta PAC	-	-	-	↑	-	-	-	-
Theta-SG PAC	-	-	-	↑	-	-	-	-
Theta-Epsilon PAC	-	-	-	-	-	-	-	↓↓
PSD steepness	-	↑↑↑↑	-	↑↑	-	↑↑	-	-
PSD offset	-	↑	-	↑↑↑↑	-	-	-	-

↑ , p < 0.05; ↑ ↑ , p < 0.01; ↑ ↑ ↑ ↑ , p < 0.0001; ↓ , p < 0.05; Mann-Whitney test

At 6 months of age both PS2APP and PS2-NI mice were characterized by sustained power levels in the Beta-Gamma frequency range, when compared to wt mice. Conversely, at the same age, wt mice showed a net, statistically significant, power decline within this frequency range with respect to 3-month-old mice (Supplementary Fig. 4A-C, H). Notably, only PS2APP mice showed an increased $1/f^x$ steepness, a property detected as early as 3 months (Fig. 2D and Supplementary Fig. 4G). Thus, the augmented spectral power correlated with the expression of the mutant PS2, whereas the increased steepness appeared to be a property linked to the expression of mutant APP. To further strengthen these linkages, we carried out similar LFP recordings in 6-month-old females from PS2KO (n = 7) (Herreman et al., 1999) and APPSwe (n = 5) (Ozmen et al., 2009) mice. As shown in Figure 6 (panels A, C), at variance with PS2-NI mice, PS2KO mice showed the same power levels of wt mice in the SG and FG ranges. Similarly, APPSwe mice, in the absence of mutant PS2, lacked the power increase in the Beta-Gamma range that characterized the PS2APP mice, while preserving the increased spectral steepness (Fig. 6B-D). Of note, at 6 months, these latter mice did not show plaques (Richards et al., 2003), yet they display intraneuronal APP/Aβ accumulation with a distribution similar to that reported for 3 month-old PS2APP mice (Supplementary Fig. 7). No power

difference was found in the other frequency bands for both PS2KO and APPSwe mice as well as in PAC and PSD offset, that resulted statistically unaltered (Supplementary Fig. 8A-H).

Taken together, the results, summarized in Table 1, indicate that the PS2APP mice express markedly different alterations of network activity in terms of Theta-Gamma frequency coupling at 3 and 6 months of age. In particular, at 6 months of age, these mice displayed significant over-coupling in two of the considered classes, as opposite to the other tg mice that reported no alteration in any class. Finally, hyper-synchronicity, as revealed by greater power steepness, characterized the early stages of PS2APP, appearing as early as 3 months and progressively declining with aging.

3.6 HIPPOCAMPAL APP PROCESSING

The hippocampi from 6-month-old APPSwe mice were also used to estimate the absolute amount of total $A\beta_{40}$ and $A\beta_{42}$, compared to PS2APP mice (see Supplementary Table 1). Upon ELISA (Millipore), we could estimate that APPSwe mice had 10 and 100 times less $A\beta_{40}$ and $A\beta_{42}$ respectively ($A\beta_{42}/A\beta_{40}$ ratio: PS2APP, 0.8; APPSwe, 0.2) while in PS2KO and PS2-NI mice Aβ was undetectable. Of note, the absolute amount of $A\beta_{42}$ in 6-month-old APPSwe mice approximated that of 3-month-old PS2APP mice (~ 100 pg/mg wet tissue). The hippocampal levels of both mouse and human full-length APP (fl-APP), as well as those of its carboxy-terminal fragments (CTFs), were analyzed by Western blotting at 6 months of age (Supplementary Methods). Both APPSwe and PS2APP mice showed large, comparable amounts of human APP (Supplementary Fig. 9A, B). The former mouse line, however, displayed much higher levels of CTFs (Supplementary Fig. 9B), as previously reported (Poirier et al., 2010). Finally, because of the mutant PS2 expression, PS2APP but not APPSwe mice had higher levels of the amyloid intracellular domain (AICD) and Aβ (Supplementary Fig. 9B). Of note, PS2-NI and PS2KO mice had mAPP levels similar to those of wt mice, however higher amounts of CTFs (Supplementary Fig. 9A, B).

4 DISCUSSION

This work was aimed at detecting, at the *in vivo* level, early alterations of spontaneous electrical activity in the homozygous PS2APP mouse model (B6.152H line), based on the two FAD-linked mutations, PS2-NI and APP Swedish (Ozmen et al., 2009). The rationale of our approach was based on the following

considerations: i) the urgency to discover early biomarkers of AD brain dysfunctions, well before the onset of amyloid deposition and the appearance of cognitive deficits, a need that is critical for both AD patient and mouse model studies; ii) the recent discovery that different PS2 mutants, including PS2-NI, exert a primary role in Ca^{2+} dyshomeostasis by causing reduced store Ca^{2+} content and increased ER-mitochondria coupling (Zampese et al., 2011a, Zampese et al., 2011b), and finally iii) the demonstration that PS2-based AD mouse models show significant early increase in neuronal Ca^{2+} excitability, at both the *in vitro* and the *in situ* level (Kipanyula et al., 2012). The latter finding thus offers the opportunity to test the "Ca^{2+} hypothesis of AD" *in vivo*, in the absence or presence of Aβ accumulation and gliosis.

To address our aim, we carried out *in vivo* LFP recordings from the two homozygous mouse lines, PS2-NI and PS2APP, as well from the prevalent background strain, the C57BL/6J (wt) mice. We acquired the LFP signal in the DG - one of the earliest affected regions - under urethane anesthesia and extracted signal features including amplitude, spectral steepness and Theta-higher frequency PAC by means of time-frequency methods. Importantly, to the end of assessing the temporal evolution of the features into exam, we investigated 3, 6 and 12 month-old female mice, i.e. before, during and after plaque deposition, and we probed the time-matched presence of histological hallmarks, in the form of amyloid plaques and astrogliosis, as well as the degree of Aβ load. As summarized in Table 1, different electrophysiological parameters were significantly altered in the two mouse lines with respect to wt mice. The physiological significance of the alterations observed in the power, PAC and steepness categories are here briefly summarized and discussed in the context of the AD neuropathology.

Similar to EEG, also LFP signals, when converted in the frequency domain by means of the Fourier transform, display a characteristic composition of a broad range of frequencies where, importantly, the amplitude exponentially decays as a function of the frequency. In agreement, the PSD function of a brain extracellular recording is often defined as $1/f^x$, where x is the scaling exponential of the decay (He et al., 2010). Recently, the $1/f^x$ function has been led down to the size of the various frequency generators (Logothetis et al., 2007) and has started to be widely recognized as a large scale representation of neural activity, thus, as a rich source of valuable information on the underlying network operations (Buzsáki et al., 2013, He et al., 2010, He, 2014).

Whereas the broad band power of extracellular brain recordings was shown to positively correlate with neuronal firing rate (Manning et al., 2009), the slope coefficient of the PSD function is a measure of neuronal firing synchronicity. In particular, a decrease in spectral steepness points to an enhancement of decoupled firing, whereas an increase in steepness indicates enhanced synchronicity (Freeman and Zhai, 2009, Podvalny et al., 2015, Voytek and Knight, 2015). In humans, aging was associated with desynchronized neural spiking activity, as measured by extracellular recordings and reflected by flatter power spectra in the semi-log space (Voytek et al., 2015).

Because PSD log-log plots, derived from LFP recordings in the DG, showed a corner frequency in the Gamma range we used the above mentioned approach to evaluate the level of synchronicity of the hippocampal network: PSD functions were thus plotted in the semi-log space and the slope coefficients were measured in the 10 – 100 Hz range, following robust linear fit (Voytek et al., 2015). An early increase of PSD steepness was already apparent at 3-months of age in PS2APP mice with respect to wt; the phenomenon persisted at 6 months, whereas a progressive reduction of its degree was observed at 12 months of age[§]. Following linear fitting, an increase in population spiking activity is also reflected by offset increase (Voytek and Knight, 2015). When compared to wt, at 3 months, PS2APP mice displayed a three times greater offset, which persisted high at 6 months of age; the offset of PS2-NI mice was not changed, however its decline was delayed.

Another notable feature of brain extracellular recordings is embodied by nested oscillations, where a slower rhythm influences a faster one in a dynamic fashion. In the last decade, this latter type of phase-amplitude CFC, known as PAC, has drawn much attention, in particular concerning the Theta and Gamma oscillations. Theta-Gamma PAC has consistently been described in several brain regions, including the cortex (Canolty et al., 2006, Lee et al., 2005) and the hippocampus (Axmacher et al., 2010, Belluscio et al., 2012, Bragin et al., 1995) and it was functionally linked to memory performance (Shirvalkar et al., 2010). Few results are available so far describing CFC in AD mouse models, at the *in vivo* level (Gurevicius et al., 2013, Ittner et al., 2014, Stoiljkovic et al., 2016).

[§] By linear fitting of PSD log-log plots in the range 30 - 100 Hz, we obtained very similar statistical differences between PS2APP and wt mice, at 3 and 6 months of age (data not shown).

We investigated the level of CFC existing in our LFP signals between the Theta phase and the amplitude of Beta, SG, FG and Epsilon band, respectively, as quantified by the GLM index. This particular feature of brain network activity is regarded as a bridge between local microscale neuronal ensembles and the systems-level macroscale network, allowing for dynamic network communication through a phase-coding mechanism (Voytek and Knight, 2015, Watrous et al., 2015).

When compared to wt, at 6 months of age, PS2APP mice displayed enhanced PAC in the Theta-Beta and -SG classes. These observations indicate a condition of over-coupling in the PS2APP line with respect to wt mice. Of note, a modest increase in Theta-Gamma coupling was also observed in 4-month-old APPSwe/PS1dE9 mice (Gurevicius et al., 2013), whereas in APP23 mice a reduction in Theta-Gamma coupling was reported (Ittner et al., 2014). In the PS2-NI line, PAC resulted unaffected with respect to wt mice in all classes, at both 3 and 6 months of age, with the two tg mouse lines reporting the strongest difference. Curiously, at 12 months of age, the observed changes in PAC were not maintained, however a decrease in Theta-Epsilon PAC was noticeable in PS2APP mice when compared to the other lines, a phenomenon that might represent the beginning of a different disease stage. A similar decrease in Theta-Gamma CFC was found in 4-month-old APP23 mice (Ittner et al., 2014).

While both the PAC and the PSD steepness are referred to as indicators of synchronicity within the network, their alterations in the PS2APP line did not overlap. It is important to note that they are not believed to represent the same phenomenon. On the one hand, PAC describes the level of modulation that the phase of a carrier frequency exerts on the amplitude of a faster one, in other words, it represents the ability of the slower rhythm to affect the statistical temporal distribution of neuronal firing. Conversely, the PSD steepness reflects the overall statistics of neuronal firing, with a steeper slope resulting from a shift of neuronal firing towards increased synchronicity, thus contributing to the power of the slower oscillations (Podvalny et al., 2015). From statistical analysis, the Theta-SG PAC significantly correlated with Theta but not Gamma power in all mouse lines, whereas a correlation between PAC and steepness was found only in PS2APP mice.

In conclusion, PSD steepness and Theta-Gamma frequency PAC are features of the hippocampal LFP signals that reliably characterize the earliest stage of the AD-like pathology in the PS2APP mouse model, and, limited to increased steepness, also the APPSwe model.

Power quantification within different frequency bands is a widely used approach. However, the physiological significance of power-content changes in a given band should be carefully addressed. The power of individual bands is estimated basing on the frequency-domain representation of the signal, i.e. the PSD function. As a matter of fact, the brain PSD is a combination of oscillatory as well as irregular activities and, as such, it is a complex and, unfortunately, poorly understood phenomenon (He, 2014). Nevertheless, general consensus advocates that while real oscillations determine narrow-band peaks in the PSD, broad-band "bulges" represent the spectral counterpart of neuronal firing.

In the present study, we observed an alteration of the PSD function in the PS2-NI and PS2APP models that occurs as a shoulder of increased power in the spectrum encompassing the Beta range in 3-month-old PS2APP mice and, respectively, the Beta-SG and the SG-FG range in the PS2APP and PS2-NI mice, at 6 months of age. The phenomenon likely reflects an increase of neuronal firing with respect to wt mice, i.e. hyper-activity, that also results in a marked increase in power offset, especially in PS2APP mice.

All in all, the here reported alterations of power spectra suggest that PS2-NI and PS2APP mouse models present a clear condition of neuronal hyper-activity at 6 months of age. Since no hyper-activity was found at the same age in PS2KO and APPSwe mice, this feature can be regarded as a gain-of-function brought about by the mutant PS2, possibly through alterations in store Ca^{2+} handling.

It remains to be established whether mutant PS2, as a cell Ca^{2+} disorganizer, exerts its effect primarily at the level of neurons or astrocytes, considered that its expression is under the prion protein promoter and the fact that astrocytes are directly involved in neuronal synchrony (Chever et al., 2016, Fellin et al., 2004, Pabst et al., 2016). While in PS2-NI mice the $A\beta_{42}$ level is very low, it is conceivable that in PS2APP mice, accumulation of $A\beta_{42}$ oligomers further contributes to hyper-activity by reducing the excitatory neuronal threshold (Busche et al., 2012, Minkeviciene et al., 2009) as well as by worsening Ca^{2+} handling (Agostini and Fasolato, 2016, Lazzari et al., 2015).

The phenomena of hyper-activity and hyper-synchronicity are both well-known in the clinical field of AD. Many works have investigated brain activity alterations in patients diagnosed with AD or MCI by means of functional imaging techniques, the most popular being the fMRI. Overall, these studies contributed to draw a picture where the beginning of the clinical phase of AD, corresponding to MCI, is marked by hyper-activity in the hippocampus as well as other cortical regions, that disappears with overt AD (Dickerson et al., 2005, Hämäläinen et al., 2007, Pihlajamaki et al., 2009). Interestingly, the here reported hippocampal hyper-activity is lost at 12 months of age while, in PS2APP mice, it was shown that defects in hippocampal working memory are present at 8 months, disappear at 12, and finally precipitate between 16 and 20 months (Woolley and Ballard, 2005).

Hyper-synchronicity, on the other hand, represents a common feature in AD, often in the form of silent seizures. The incidence of seizures is higher in AD patients than in control groups (Lozsadi and Larner, 2006) and it reaches even higher levels in the early-onset FAD subjects (Palop and Mucke, 2009) with 32% of PS2-N141I-FAD patients showing seizures (Jayadev et al., 2010). Notably, epileptic events have been often observed as electroencephalographic seizures associated with transient epileptic amnesia (TEA) (Rabinowicz et al., 2000), raising the hypothesis of epileptic discharge to be an underestimated phenomenon (Mendes, 2002, Palop et al., 2007).

Taken together, the above described findings provide a framework for the interpretation of our results in regard to both hyper-excitability and hyper-synchronicity. The former, that we statistically detect in both PS2-NI and PS2APP lines at 6 months of age, is in line with previous studies indicating a condition of enhanced fMRI activity in MCI patients, while the latter correlates with higher incidence of epilepsy found in FAD families' pedigrees, as well as with the consistent observation of TEA in AD patients.

The neuronal hyper-activity, found in both the above mentioned tg lines, adds to similar previous observations obtained from other AD mouse models, in support to the hypothesis claiming early neuronal hyper-activity to be a biomarker of AD. In particular, neuronal hyper-excitability was demonstrated in mouse models expressing human FAD-linked APP mutations alone or together with different PS1 mutations and it was linked to the appearance of non-convulsive seizures (Palop et al., 2007). Epileptic activity has been consistently found in APPJ20 (Palop et al., 2007), APP23 (Ittner et al., 2014), Tg2576 (Westmark et al.,

435 2008) and CRND8 mice (Del Vecchio et al., 2004). In particular, not only sporadic seizures were described to
436 spontaneously appear in freely behaving animals (Ittner et al., 2014, Palop et al., 2007, Westmark et al.,
437 2008) but, in addition, hyper-synchronicity emerged as an enhanced tendency to the development of
438 seizures after administration of riluzole (Ittner et al., 2014, Verret et al., 2012), a voltage gated sodium
439 channel blocker, or pentylenetetrazol (Del Vecchio et al., 2004, Westmark et al., 2008), a GABA-A receptor
440 antagonist.
441 Hyper-activity, in terms of increased neuronal firing rate, was reported in 4- to 7-month-old APPJ20 mice
442 under basal conditions, just before plaque deposition (Verret et al., 2012). Higher seizure susceptibility and
443 hyper-synchrony were reported in Tg2576 mice as early as 1.5 months (Bezzina et al., 2015), as well as in
444 APPSwe/PS1dE9, a line that, for some features, resembles the PS2APP line: i.e. similar $A\beta_{42}$, $A\beta_{40}$ levels and
445 ratio (Gurevicius et al., 2013, Minkeviciene et al., 2009, Sierksma et al., 2013) and, possibly, also store Ca^{2+}
446 deficit (Honarnejad et al., 2013), but differs for the larger and wider expression of hAPPSwe, being also this
447 latter under the prion protein promoter.
448 Furthermore, neuronal hyper-activity, as augmented rate of Ca^{2+} transients, was observed in the cortex of
449 6-month-old mice from the APP23xPS45 line (Busche et al., 2008), and was later reported to occur in the
450 hippocampus as well, at the age of 1-2 months, before plaque deposition (Busche et al., 2012). Close to our
451 study, enhancement of hippocampal Gamma power in the range ~ 20-45 Hz was reported in freely
452 behaving 4-month-old APP23 mice (Ittner et al., 2014), characterized by plaque deposition starting at 6
453 months of age (Sturchler-Pierrat et al., 1997).
454 To address the question of what, among Ca^{2+} hyper-activity, APP overexpression, or Aβ accumulation, is the
455 major responsible of the observed phenomena, we compared PS2APP mice with the mouse lines carrying
456 the single mutations. Interestingly, PS2APP mice develop a condition of hippocampal hyper-activity at the
457 same age of PS2-NI mice. This occurs despite the drastically different levels of Aβ production. In particular,
458 at 6 months, when we found increased SG-FG power, PS2-NI mice present neither plaque deposition nor
459 significant signs of astrogliosis, with $A\beta_{42}$ levels not significantly higher than those found in age-matched wt
460 mice. Thus, hyper-activity in the Gamma band does not seem to correlate with $A\beta_{42}$ levels and, considering
461 the mismatch with plaques and astrogliosis in PS2-NI mice, it is not due to a compensatory mechanism

(Stargardt et al., 2015). Finally, this type of hyper-activity was absent in 6-month-old PS2KO and APPSwe mice, despite these latter reach $A\beta_{42}$ levels in the range of the 3-month-old PS2APP mice. Altogether these findings reinforce the idea that hyper-activity likely represents a gain-of-function, due to the mutant PS2. Nevertheless, when compared to PS2-NI, PS2APP mice exhibit a pattern of alterations of the LFP activity that is more complex. Indeed, in conjunction with the hyper-activity, they also present hyper-synchronicity, detectable as early as 3 months of age in the form of a steeper PSD function decay, and, at 6 months of age, as an enhanced Theta-Beta and Theta-SG PAC. Since hyper-synchronicity is not detectable in the PS2-NI line at any age, this aspect was possibly attributable to the much higher levels of soluble Aβ. Experiments on 6-month-old APPSwe mice confirmed the presence of hyper-synchronicity, however in the absence of PAC alterations, i.e. a condition similar to that found in 3-month-old PS2APP. These findings indicate that an increase in power steepness is required but not sufficient to observe Theta-SG PAC and support the hypothesis of an enhanced neuronal activity, in the form of hyper-synchronicity, preceding the first histo-pathological and clinical symptoms (Stargardt et al., 2015). The observed phenomena are consistent with the sharp wave discharge found in Tet-Off APP mice, a type of hyper-synchronization that could be rescued by APP suppression (Born et al., 2014). Whether the here described hyper-synchronicity is due to fl-APP or one of its products has to be tested yet. Indeed, with respect to APPSwe, PS2APP mice show almost similar levels of fl-APP albeit a much larger amount of CTFs and AICD, thus, accumulation of these latter might play the major role. It is worth noting that disruption of Theta-FG CFC was observed in hippocampus, but not prefrontal cortex, of APP-KO mice, in the absence of specific effects on oscillation power (Zhang et al., 2016), thus suggesting that endogenous APP plays a direct role on regional coupling mechanisms. Finally, the increase in PAC, which we observed only in 6-month-old PS2APP mice, well correlates with the rising phase of $A\beta_{42}$ accumulation and gliosis.

It is worth mentioning that hyper-activity at the DG level has been connected to reduced neurogenesis given that DG interneurons seem to be more effectively driven by young adult-born neurons (Lacefield et al., 2012). Of note, the PS2APP mice are characterized by reduced neurogenesis at the DG level as early as 4 months of age (Poirier et al., 2010, Richards et al., 2003).

Because homozygous tg mice were used in this study, we cannot entirely exclude that genetic drift might have occurred in our colonies, however we can reasonably rule out that, the two principal features, i.e. the increase in the broad band Gamma power and the increase in steepness were due to genetic drift. In fact, it is highly unlikely that they similarly occurred in two different tg lines, the PS2-NI and PS2APP mice, from one side, and the PS2APP and APPSwe mice, from the other.

Although many studies have pointed to an increased spiking synchronicity as a common feature of mouse lines expressing mutated forms of APP, to the best of our knowledge, no previous report with AD mouse models addressed neuronal synchronicity by means of the PSD steepness. By means of this tool, we were able to distinguish the specific contribution of mutant PS2 and APP to early hippocampal network dysfunctions.

5 CONCLUSIONS

In the DG of PS2APP mice, we report three major patterns of early electrophysiological alterations: i) increased power in the Beta/Gamma frequency bands; ii) increased power steepness; iii) increased PAC in the Theta-Beta and Theta-SG bands. The first two findings can be attributed to the expression of mutant PS2 and APP, respectively. Only the appearance of increased PAC uniquely characterizes the PS2APP mice at 6 months of age when plaques and gliosis start to appear.

6 ACKNOWLEDGEMENTS

We are grateful to L. Ozmen and F. Hoffmann-La Roche Ltd (Basel, Switzerland) for kindly donating the PS2APP and APPSwe mice, to T. Pozzan and P. Magalhaes for support and critical reading the manuscript. This work was supported by the Italian Ministry of University and Scientific Research and the University of Padua (FASO-PRAT16-01 to CF); FINA grant to SV; the Strategic Projects of the University of Padua and the Italian National Research Council, CNR (Ageing project to TP); RF, MR and MA were supported by a Ph.D. fellowship from the University of Padua. ES was a graduate student of the University of Padua, RF and EM and MM, as post-docs, were supported by FINA grant to SV. We declare no competing financial interests.

Author statement: CF, RF and SV planned and designed the work; RF and CF wrote the manuscript; RF and EM (partial contribution) executed the electrophysiological experiments; MM, RF, MR and GS performed analyses on electrophysiological data; MA and ES executed the histology and the biochemical experiments.

ACCEPTED MANUSCRIPT

7 DISCLOSURE STATEMENT

The authors declare no conflicts of interest.

ACCEPTED MANUSCRIPT

8 REFERENCES

Agostini, M., Fasolato, C., 2016. When, where and how? Focus on neuronal calcium dysfunctions in Alzheimer's Disease. Cell Calcium.

Axmacher, N., Henseler, M.M., Jensen, O., Weinreich, I., Elger, C.E., Fell, J., 2010. Cross-frequency coupling supports multi-item working memory in the human hippocampus. Proc.Natl.Acad.Sci.U.S.A. 107, 3228-3233.

Belluscio, M.A., Mizuseki, K., Schmidt, R., Kempter, R., Buzsaki, G., 2012. Cross-frequency phase-phase coupling between theta and gamma oscillations in the hippocampus. J.Neurosci. 32, 423-435.

Bezzina, C., Verret, L., Juan, C., Remaud, J., Halley, H., Rampon, C., Dahan, L., 2015. Early onset of hypersynchronous network activity and expression of a marker of chronic seizures in the Tg2576 mouse model of Alzheimer's disease. 10, e0119910.

Bhat, S., Acharya, U.R., Dadmehr, N., Adeli, H., 2015. Clinical Neurophysiological and Automated EEG-Based Diagnosis of the Alzheimer's Disease. Eur.Neurol. 74, 202-210.

Born, H.A., Kim, J.Y., Savjani, R.R., Das, P., Dabaghian, Y.A., Guo, Q., Yoo, J.W., Schuler, D.R., Cirrito, J.R., Zheng, H., Golde, T.E., Noebels, J.L., Jankowsky, J.L., 2014. Genetic suppression of transgenic APP rescues Hypersynchronous network activity in a mouse model of Alzeimer's disease. J.Neurosci. 34, 3826-3840.

Bragin, A., Jando, G., Nadasdy, Z., Hetke, J., Wise, K., Buzsaki, G., 1995. Gamma (40-100 Hz) oscillation in the hippocampus of the behaving rat. J.Neurosci. 15, 47-60.

Busche, M.A., Grienberger, C., Keskin, A.D., Song, B., Neumann, U., Staufenbiel, M., Förstl, H., Konnerth, A., 2015. Decreased amyloid-[beta] and increased neuronal hyperactivity by immunotherapy in Alzheimer's models. Nat.Neurosci.

Busche, M.A., Chen, X., Henning, H.A., Reichwald, J., Staufenbiel, M., Sakmann, B., Konnerth, A., 2012. Critical role of soluble amyloid-beta for early hippocampal hyperactivity in a mouse model of Alzheimer's disease. Proc.Natl.Acad.Sci.U.S.A. 109, 8740-8745.

Busche, M.A., Eichhoff, G., Adelsberger, H., Abramowski, D., Wiederhold, K.H., Haass, C., Staufenbiel, M., Konnerth, A., Garaschuk, O., 2008. Clusters of hyperactive neurons near amyloid plaques in a mouse model of Alzheimer's disease. Science. 321, 1686-1689.

Buzsáki, G., Logothetis, N., Singer, W., 2013. Scaling brain size, keeping timing: evolutionary preservation of brain rhythms. Neuron. 80, 751-764.

Camandola, S., Mattson, M.P., 2011. Aberrant subcellular neuronal calcium regulation in aging and Alzheimer's disease. 1813, 965-973.

Canolty, R.T., Edwards, E., Dalal, S.S., Soltani, M., Nagarajan, S.S., Kirsch, H.E., Berger, M.S., Barbaro, N.M., Knight, R.T., 2006. High gamma power is phase-locked to theta oscillations in human neocortex. Science. 313, 1626-1628.

Chever, O., Dossi, E., Pannasch, U., Derangeon, M., Rouach, N., 2016. Astroglial networks promote neuronal coordination. Sci.Signal. 9, ra6.

556 Decuypere, J., Bultynck, G., Parys, J.B., 2011. A dual role for Ca 2 in autophagy regulation. Cell
557 Calcium. 50, 242-250.

558 Del Vecchio, R.A., Gold, L.H., Novick, S.J., Wong, G., Hyde, L.A., 2004. Increased seizure
559 threshold and severity in young transgenic CRND8 mice. Neurosci.Lett. 367, 164-167.

560 Dickerson, B.C., Salat, D.H., Greve, D.N., Chua, E.F., Rand-Giovannetti, E., Rentz, D.M., Bertram,
561 L., Mullin, K., Tanzi, R.E., Blacker, D., Albert, M.S., Sperling, R.A., 2005. Increased hippocampal
562 activation in mild cognitive impairment compared to normal aging and AD. Neurology. 65, 404-
563 411.

564 Fellin, T., Pascual, O., Gobbo, S., Pozzan, T., Haydon, P.G., Carmignoto, G., 2004. Neuronal
565 synchrony mediated by astrocytic glutamate through activation of extrasynaptic NMDA receptors.
566 Neuron. 43, 729-743.

567 Freeman, W.J., Zhai, J., 2009. Simulated power spectral density (PSD) of background
568 electrocorticogram (ECoG). 3, 97-103.

569 Giacomello, M., Barbiero, L., Zatti, G., Squitti, R., Binetti, G., Pozzan, T., Fasolato, C., Ghidoni,
570 R., Pizzo, P., 2005. Reduction of Ca 2 stores and capacitative Ca 2 entry is associated with the
571 familial Alzheimer's disease presenilin-2 T122R mutation and anticipates the onset of dementia.
572 Neurobiol.Dis. 18, 638-648.

573 Golde, T.E., Schneider, L.S., Koo, E.H., 2011. Anti-aβ therapeutics in Alzheimer's disease: the need
574 for a paradigm shift. Neuron. 69, 203-213.

575 Gurevicius, K., Lipponen, A., Tanila, H., 2013. Increased cortical and thalamic excitability in freely
576 moving APPswe/PS1dE9 mice modeling epileptic activity associated with Alzheimer's disease.
577 Cereb.Cortex. 23, 1148-1158.

578 Hämäläinen, A., Pihlajamäki, M., Tanila, H., Hänninen, T., Niskanen, E., Tervo, S., Karjalainen,
579 P.A., Vanninen, R.L., Soininen, H., 2007. Increased fMRI responses during encoding in mild
580 cognitive impairment. Neurobiol.Aging. 28, 1889-1903.

581 He, B.J., 2014. Scale-free brain activity: past, present, and future. Trends Cogn.Sci.(Regul.Ed.). 18,
582 480-487.

583 He, B.J., Zempel, J.M., Snyder, A.Z., Raichle, M.E., 2010. The temporal structures and functional
584 significance of scale-free brain activity. Neuron. 66, 353-369.

585 Herreman, A., Hartmann, D., Annaert, W., Saftig, P., Craessaerts, K., Serneels, L., Umans, L.,
586 Schrijvers, V., Checler, F., Vanderstichele, H., Baekelandt, V., Dressel, R., Cupers, P.,
587 Huylebroeck, D., Zwijsen, A., Van Leuven, F., De Strooper, B., 1999. Presenilin 2 deficiency
588 causes a mild pulmonary phenotype and no changes in amyloid precursor protein processing but
589 enhances the embryonic lethal phenotype of presenilin 1 deficiency. Proc.Natl.Acad.Sci.U.S.A. 96,
590 11872-11877.

591 Honarnejad, K., Jung, C.K., Lammich, S., Arzberger, T., Kretzschmar, H., Herms, J., 2013.
592 Involvement of presenilin holoprotein upregulation in calcium dyshomeostasis of Alzheimer's
593 disease. J.Cell.Mol.Med. 17, 293-302.

594 Huang, Y., Yang, S., Hu, Z., Liu, G., Zhou, W., Zhang, Y., 2012. A new approach to location of the
595 dentate gyrus and perforant path in rats/mice by landmarks on the skull. 72, 468-472.

Ittner, A.A., Gladbach, A., Bertz, J., Suh, L.S., Ittner, L.M., 2014. p38 MAP kinase-mediated NMDA receptor-dependent suppression of hippocampal hypersynchronicity in a mouse model of Alzheimer's disease. 2, 1-17.

Jayadev, S., Leverenz, J.B., Steinbart, E., Stahl, J., Klunk, W., Yu, C.E., Bird, T.D., 2010. Alzheimer's disease phenotypes and genotypes associated with mutations in presenilin 2. Brain. 133, 1143-1154.

Khan, U.A., Liu, L., Provenzano, F.A., Berman, D.E., Profaci, C.P., Sloan, R., Mayeux, R., Duff, K.E., Small, S.A., 2014. Molecular drivers and cortical spread of lateral entorhinal cortex dysfunction in preclinical Alzheimer's disease. Nat.Neurosci. 17, 304-311.

Kipanyula, M.J., Contreras, L., Zampese, E., Lazzari, C., Wong, A.K., Pizzo, P., Fasolato, C., Pozzan, T., 2012. Ca2 dysregulation in neurons from transgenic mice expressing mutant presenilin 2. 11, 885-893.

Lacefield, C.O., Itskov, V., Reardon, T., Hen, R., Gordon, J.A., 2012. Effects of adult ‐ generated granule cells on coordinated network activity in the dentate gyrus. Hippocampus. 22, 106-116.

Lazzari, C., Kipanyula, M.J., Agostini, M., Pozzan, T., Fasolato, C., 2015. Aβ42 oligomers selectively disrupt neuronal calcium release. Neurobiol.Aging. 36, 877-885.

Lee, H., Simpson, G.V., Logothetis, N.K., Rainer, G., 2005. Phase locking of single neuron activity to theta oscillations during working memory in monkey extrastriate visual cortex. Neuron. 45, 147-156.

Logothetis, N.K., Kayser, C., Oeltermann, A., 2007. In vivo measurement of cortical impedance spectrum in monkeys: implications for signal propagation. Neuron. 55, 809-823.

Lord, A., Kalimo, H., Eckman, C., Zhang, X., Lannfelt, L., Nilsson, L.N., 2006. The Arctic Alzheimer mutation facilitates early intraneuronal Aβ aggregation and senile plaque formation in transgenic mice. Neurobiol.Aging. 27, 67-77.

Lozsadi, D.A., Larner, A.J., 2006. Prevalence and causes of seizures at the time of diagnosis of probable Alzheimer's disease. Dement.Geriatr.Cogn.Disord. 22, 121-124.

Manning, J.R., Jacobs, J., Fried, I., Kahana, M.J., 2009. Broadband shifts in local field potential power spectra are correlated with single-neuron spiking in humans. J.Neurosci. 29, 13613-13620.

Mendes, M.H.F., 2002. Transient epileptic amnesia: an under-diagnosed phenomenon? Three more cases. Seizure. 11, 238-242.

Minkeviciene, R., Rheims, S., Dobszay, M.B., Zilberter, M., Hartikainen, J., Fulop, L., Penke, B., Zilberter, Y., Harkany, T., Pitkanen, A., Tanila, H., 2009. Amyloid beta-induced neuronal hyperexcitability triggers progressive epilepsy. J.Neurosci. 29, 3453-3462.

Mitchell, A.J., Monge-Argiles, J.A., Sanchez-Paya, J., 2010. Do CSF biomarkers help clinicians predict the progression of mild cognitive impairment to dementia?. Pract.Neurol. 10, 202-207.

Namgung, U., Valcourt, E., Routtenberg, A., 1995. Long-term potentiation in vivo in the intact mouse hippocampus. Brain Res. 689, 85-92.

633 Ozmen, L., Albientz, A., Czech, C., Jacobsen, H., 2009. Expression of transgenic APP mRNA is
634 the key determinant for beta-amyloid deposition in PS2APP transgenic mice. Neurodegener Dis. 6,
635 29-36.

636 Pabst, M., Braganza, O., Dannenberg, H., Hu, W., Pothmann, L., Rosen, J., Mody, I., van Loo, K.,
637 Deisseroth, K., Becker, A.J., 2016. Astrocyte Intermediaries of Septal Cholinergic Modulation in
638 the Hippocampus. Neuron. 90, 853-865.

639 Palop, J.J., Chin, J., Roberson, E.D., Wang, J., Thwin, M.T., Bien-Ly, N., Yoo, J., Ho, K.O., Yu,
640 G., Kreitzer, A., 2007. Aberrant excitatory neuronal activity and compensatory remodeling of
641 inhibitory hippocampal circuits in mouse models of Alzheimer's disease. Neuron. 55, 697-711.

642 Palop, J.J., Mucke, L., 2009. Epilepsy and cognitive impairments in Alzheimer disease.
643 Arch.Neurol. 66, 435-440.

644 Penny, W., Duzel, E., Miller, K., Ojemann, J., 2008. Testing for nested oscillation.
645 J.Neurosci.Methods. 174, 50-61.

646 Pihlajamaki, M., Jauhiainen, A.M., Soininen, H., 2009. Structural and functional MRI in mild
647 cognitive impairment. 6, 179-185.

648 Podvalny, E., Noy, N., Harel, M., Bickel, S., Chechik, G., Schroeder, C.E., Mehta, A.D., Tsodyks,
649 M., Malach, R., 2015. A unifying principle underlying the extracellular field potential spectral
650 responses in the human cortex. J.Neurophysiol., jn. 00943.2014.

651 Poirier, R., Veltman, I., Pflimlin, M.C., Knoflach, F., Metzger, F., 2010. Enhanced dentate gyrus
652 synaptic plasticity but reduced neurogenesis in a mouse model of amyloidosis. Neurobiol.Dis. 40,
653 386-393.

654 Prendergast, B.J., Onishi, K.G., Zucker, I., 2014. Female mice liberated for inclusion in
655 neuroscience and biomedical research. 40, 1-5.

656 Rabinowicz, A.L., Starkstein, S.E., Leiguarda, R.C., Coleman, A.E., 2000. Transient epileptic
657 amnesia in dementia: a treatable unrecognized cause of episodic amnestic wandering. 14, 231-233.

658 Richards, J.G., Higgins, G.A., Ouagazzal, A.M., Ozmen, L., Kew, J.N., Bohrmann, B., Malherbe,
659 P., Brockhaus, M., Loetscher, H., Czech, C., Huber, G., Bluethmann, H., Jacobsen, H., Kemp, J.A.,
660 2003. PS2APP transgenic mice, coexpressing hPS2mut and hAPPswe, show age-related cognitive
661 deficits associated with discrete brain amyloid deposition and inflammation. J.Neurosci. 23, 8989-
662 9003.

663 Shirvalkar, P.R., Rapp, P.R., Shapiro, M.L., 2010. Bidirectional changes to hippocampal theta-
664 gamma comodulation predict memory for recent spatial episodes. Proc.Natl.Acad.Sci.U.S.A. 107,
665 7054-7059.

666 Sierksma, A.S., Rutten, K., Sydlik, S., Rostamian, S., Steinbusch, H.W., van den Hove, Daniel LA,
667 Prickaerts, J., 2013. Chronic phosphodiesterase type 2 inhibition improves memory in the
668 APPswe/PS1dE9 mouse model of Alzheimer's disease. Neuropharmacology. 64, 124-136.

669 Stargardt, A., Swaab, D.F., Bossers, K., 2015. The storm before the quiet: neuronal hyperactivity
670 and Aβ in the presymptomatic stages of Alzheimer's disease. Neurobiol.Aging. 36, 1-11.

671 Steardo Jr, L., Bronzuoli, M.R., Iacomino, A., Esposito, G., Steardo, L., Scuderi, C., 2015. Does
672 neuroinflammation turn on the flame in Alzheimer's disease? Focus on astrocytes. 9.

673 Stoiljkovic, M., Kelley, C., Hajós, G.P., Nagy, D., Koenig, G., Leventhal, L., Hajós, M., 2016.
674 Hippocampal network dynamics in response to α7 nACh receptors activation in amyloid-β
675 overproducing transgenic mice. Neurobiol.Aging.

676 Sturchler-Pierrat, C., Abramowski, D., Duke, M., Wiederhold, K.H., Mistl, C., Rothacher, S.,
677 Ledermann, B., Burki, K., Frey, P., Paganetti, P.A., Waridel, C., Calhoun, M.E., Jucker, M., Probst,
678 A., Staufenbiel, M., Sommer, B., 1997. Two amyloid precursor protein transgenic mouse models
679 with Alzheimer disease-like pathology. Proc.Natl.Acad.Sci.U.S.A. 94, 13287-13292.

680 Verret, L., Mann, E.O., Hang, G.B., Barth, A.M., Cobos, I., Ho, K., Devidze, N., Masliah, E.,
681 Kreitzer, A.C., Mody, I., 2012. Inhibitory interneuron deficit links altered network activity and
682 cognitive dysfunction in Alzheimer model. Cell. 149, 708-721.

683 Voytek, B., Knight, R.T., 2015. Dynamic network communication as a unifying neural basis for
684 cognition, development, aging, and disease. Biol.Psychiatry. 77, 1089-1097.

685 Voytek, B., Kramer, M.A., Case, J., Lepage, K.Q., Tempesta, Z.R., Knight, R.T., Gazzaley, A.,
686 2015. Age-Related Changes in 1/f Neural Electrophysiological Noise. J.Neurosci. 35, 13257-13265.

687 Watrous, A.J., Deuker, L., Fell, J., Axmacher, N., 2015. Phase-amplitude coupling supports phase
688 coding in human ECoG. Elife. 4, 10.7554/eLife.07886.

689 Westmark, C.J., Westmark, P.R., Beard, A.M., Hildebrandt, S.M., Malter, J.S., 2008. Seizure
690 susceptibility and mortality in mice that over-express amyloid precursor protein.
691 Int.J.Clin.Exp.Pathol. 1, 157-168.

692 Woolley, M., Ballard, T., 2005. Age-related impairments in operant DMTP performance in the
693 PS2APP mouse, a transgenic mouse model of Alzheimer's disease. Behav.Brain Res. 161, 220-228.

694 World Health Organization, 2015. Fact sheet N°362, March 2015.

695 Xu, W., Fitzgerald, S., Nixon, R.A., Levy, E., Wilson, D.A., 2015. Early hyperactivity in lateral
696 entorhinal cortex is associated with elevated levels of AβPP metabolites in the Tg2576 mouse
697 model of Alzheimer's disease. Exp.Neurol. 264, 82-91.

698 Zampese, E., Fasolato, C., Pozzan, T., Pizzo, P., 2011a. Presenilin-2 modulation of ER-
699 mitochondria interactions: FAD mutations, mechanisms and pathological consequences. 4, 357-360.

700 Zampese, E., Fasolato, C., Kipanyula, M.J., Bortolozzi, M., Pozzan, T., Pizzo, P., 2011b. Presenilin
701 2 modulates endoplasmic reticulum (ER)-mitochondria interactions and Ca2+ cross-talk.
702 Proc.Natl.Acad.Sci.U.S.A. 108, 2777-2782.

703 Zatti, G., Burgo, A., Giacomello, M., Barbiero, L., Ghidoni, R., Sinigaglia, G., Florean, C., Bagnoli,
704 S., Binetti, G., Sorbi, S., 2006. Presenilin mutations linked to familial Alzheimer's disease reduce
705 endoplasmic reticulum and Golgi apparatus calcium levels. Cell Calcium. 39, 539-550.

706 Zhang, X., Zhong, W., Brankack, J., Weyer, S.W., Muller, U.C., Tort, A.B., Draguhn, A., 2016.
707 Impaired theta-gamma coupling in APP-deficient mice. Sci.Rep. 6, 21948.

ACCEPTED MANUSCRIPT

708 Zou, C., Montagna, E., Shi, Y., Peters, F., Blazquez-Llorca, L., Shi, S., Filser, S., Dorostkar, M.M.,
709 Herms, J., 2015. Intraneuronal APP and extracellular Aβ independently cause dendritic spine
710 pathology in transgenic mouse models of Alzheimer's disease. Acta Neuropathol. 129, 909-920.

711
712

ACCEPTED MANUSCRIPT

9 FIGURE LEGENDS

Figure 1. Power spectra of LFP signals recorded in vivo from the DG of wt, PS2-NI and PS2APP mice. *Left:* frequency distribution obtained as described in Methods at 3 (A), 6 (B) and 12 (C) months of age (mean, continuous line; SEM, dotted line, for legibility only one SEM is shown); *insets*, magnifications highlighting the Beta-Gamma frequency range. *Right:* Bars represent the average power at 3, 6 and 12 months of age for each genotype within the following discrete bands: Beta, 10 - 15 Hz (D), SG, 25 – 40 Hz (E) and FG, 40 – 90 Hz (F); mean ± SEM, n =11, 8, 8 (3-months); 10, 12, 12 (6-months) and 9, 7, 9 (12-months) for wt, PS2-NI and PS2APP mice respectively; * $p < 0.05$; ** $p < 0.01$; Mann-Whitney rank-sum test. Unless specified, the mouse number is the same for all the other figures.

Figure 2. Linear fitting of PSD from wt, PS2-NI and PS2APP mice. (A-C) The mean power spectrum of each genotype at 3, 6 and 12 months of age, obtained as shown in Figure 1, is reported along with the linear fitting (straight line) in the semi-log space. (D,E) Bar graphs summarizing the mean linear-fit slope coefficient (D) and the offset (E) in the range 10-100 Hz. Mean ± SEM; ° $p = 0.06$ * $p < 0.05$; ** $p < 0.01$; *** $p < 0.001$; **** $p < 0.0001$; Mann-Whitney rank-sum test.

Figure 3. Analysis of Theta-higher frequency bands PAC. (A-D) Bar graphs report the mean PAC index (GLM) within the Theta-Beta (A), Theta-SG (B), Theta-FG (C) and Theta-Epsilon (D) classes for wt, PS2-NI and PS2APP mice at different ages. Mean ± SEM for wt, PS2-NI and PS2APP lines respectively; * $p < 0.05$; ** $p < 0.01$; Mann-Whitney rank-sum test.

Figure 4. Plaque deposition and astrogliosis in wt, PS2-NI and PS2APP mice. (A-C) Representative images of immunostaining for APP/Aβ with 4G8 (left) and astrogliosis with GFAP (right), obtained as described in Methods from wt (**A**), PS2-NI (**B**) and PS2APP (**C**) mice (Scale bar, 300 µm). (D) Bar graph represents the astrocyte reactivity evaluated on the basis of the GFAP staining intensity within the sub-regions indicated in panel A (dashed lines). CA, Cornu Ammonis; DG, Dentate Gyrus; Sb, Subiculum; scale bar, 300 µm. Mean ± SEM n = 3-4 animals (3 slices each) per genotype; * $p < 0.05$; Mann-Whitney rank-sum test.

Figure 5. Intraneuronal APP/Aβ accumulation in 3-month-old PS2APP mice. (A) Representative image of APP/Aβ immunostaining (4G8) of sagittal hippocampal sections from 3-month-old PS2APP mice. Intracellular APP/Aβ accumulation is particularly strong in CA1 pyramidal layer and in the subiculum. Scale

740 bar, 300 µm. (B) Magnification (5x) of the subiculum region shown in A; n = 3 PS2APP mice (3 slices each).
741 (C) Representative image of a 100x acquisition of the subiculum region co-stained for APP/Aβ and GFAP.
742 Scale bar, 20 µm.

743 **Figure 6. PSD and steepness in PS2KO and APPSwe mice.** (A,B) PSD functions in the log-log (A) and semi-
744 log (B) space of wt (replicated from Figs. 1 and 2), PS2KO and APPSwe mice at 6 months of age (mean,
745 continuous line; SEM, dotted line, for legibility only one SEM is shown). Straight lines in B represent PSD
746 linear fittings. (C,D) The bar graphs report the mean power quantified in the Beta, SG and FG bands (C), and
747 the mean linear-fit slope coefficient (D), measured in 6 month-old wt, PS2KO and APPSwe mice. Mean ± SEM,
748 n = 10, 7, 5 for wt, PS2KO and APPSwe mice respectively; ** $p < 0.01$; Mann-Whitney rank-sum test.

ACCEPTED MANUSCRIPT

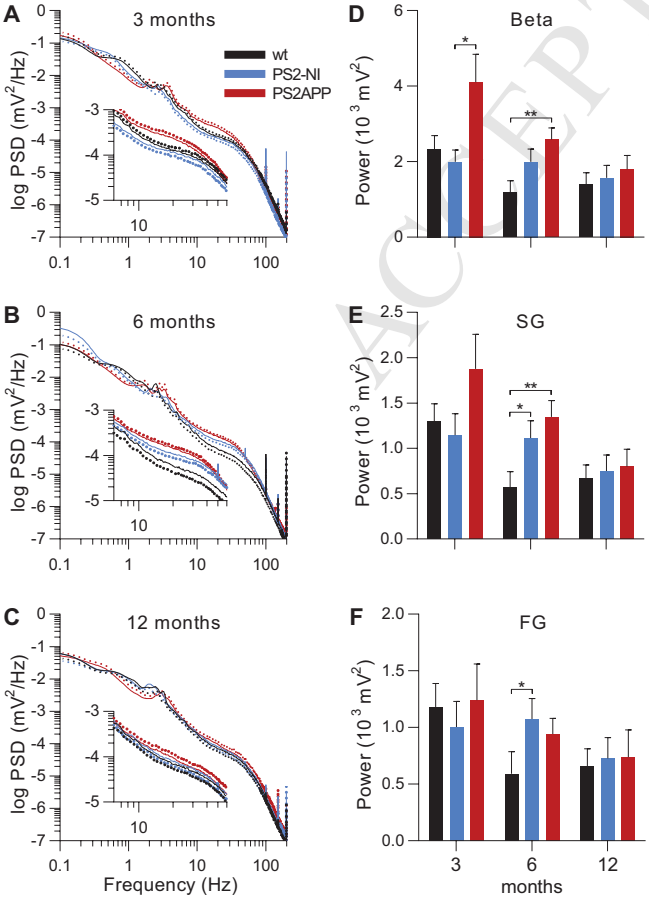

ACCEPTED MANUSCRIPT

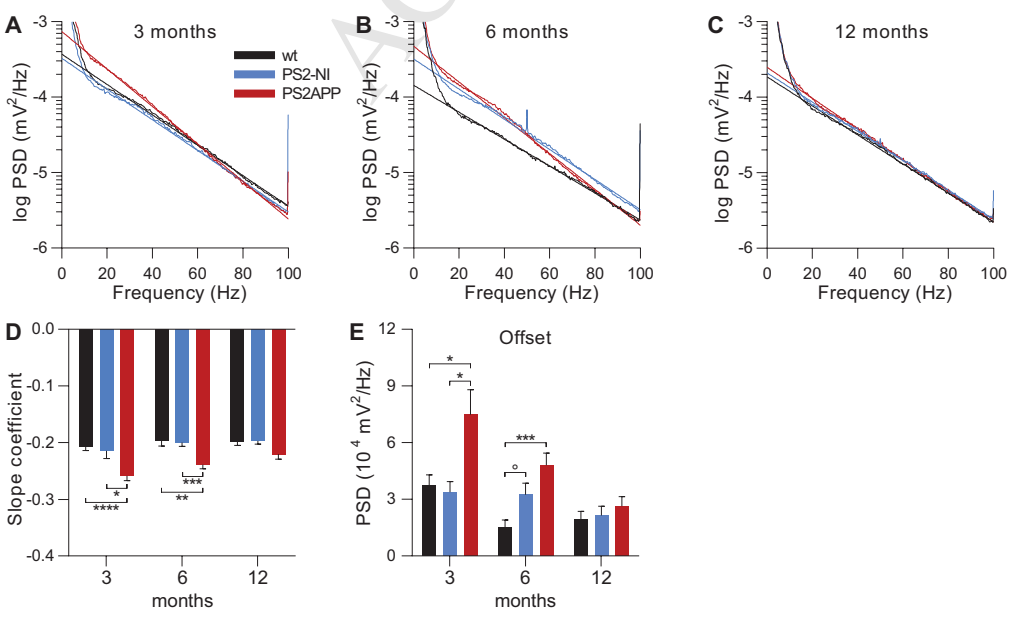

ACCEPTED MANUSCRIPT

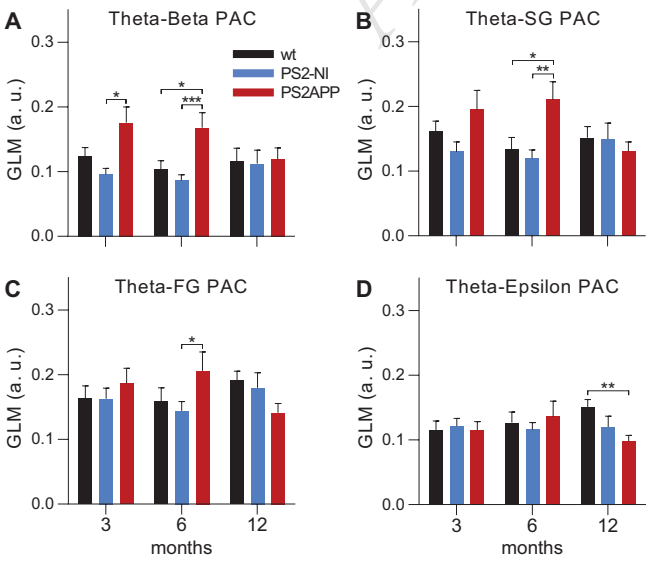

ACCEPTED MANUSCRIPT

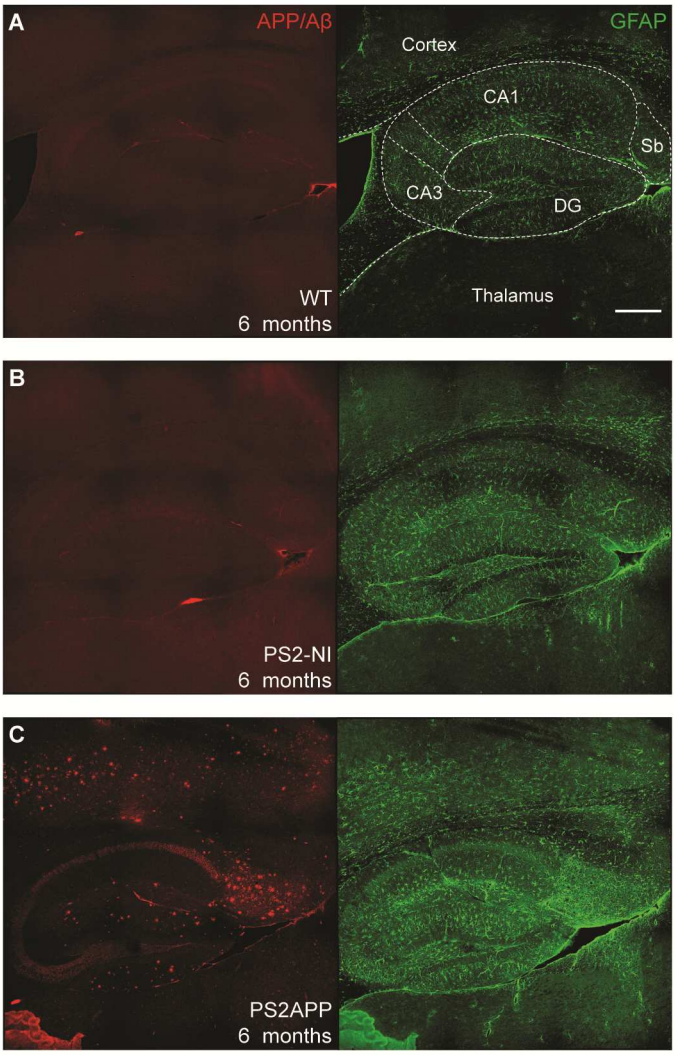

ACCEPTED MANUSCRIPT

ACCEPTED MANUSCRIPT

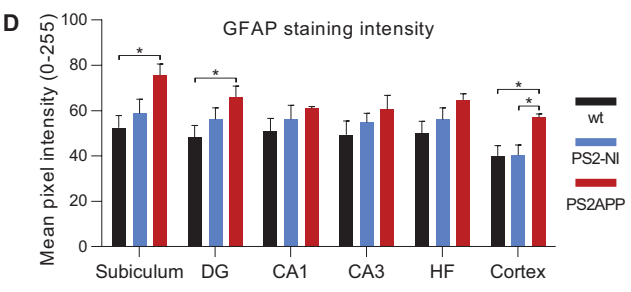

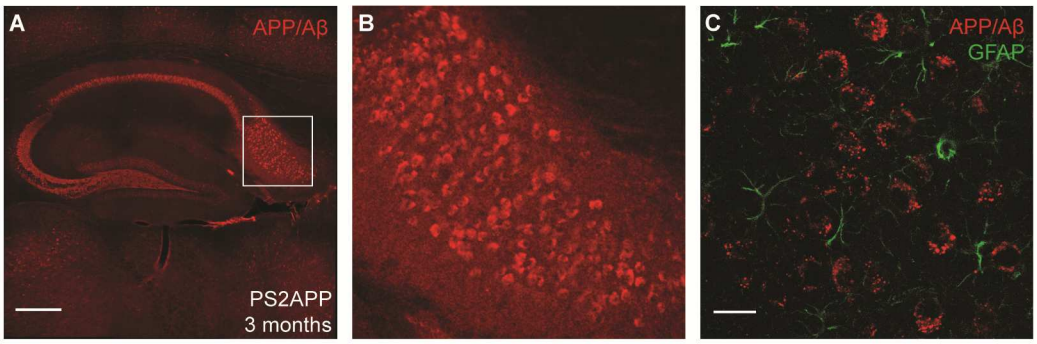

ACCEPTED MANUSCRIPT

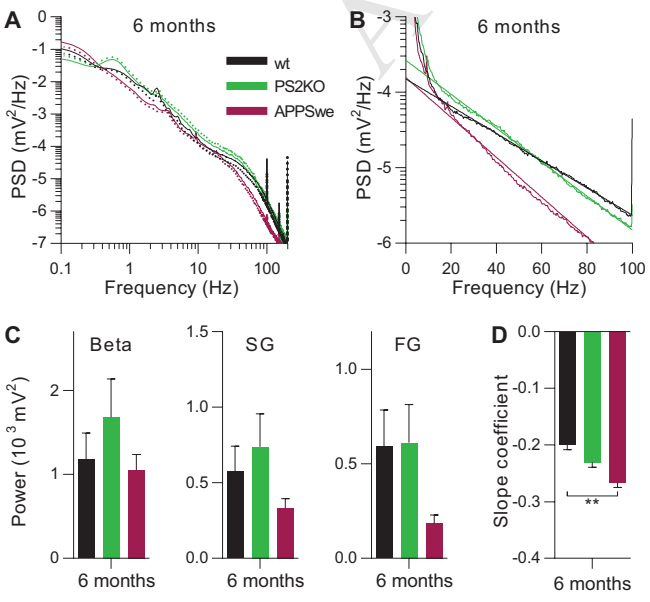

ACCEPTED MANUSCRIPT

ACCEPTED MANUSCRIPT

HIGHLIGHTS

- In vivo spontaneous LFP activity in dentate gyrus of PS2-based AD mouse models.
- Enhanced Beta/Gamma power and spectral steepness early characterize PS2APP mice.
- The spectral steepness increase anticipates plaque deposition and gliosis.
- Power increase and CFC enhancement timely occur with AD histo-pathological traits.
- Power and steepness increases are associated with mutant PS2 and APP, respectively.

ACCEPTED MANUSCRIPT